

Add force and/or change underlying projection method
to improve accuracy of Explicit Robin-Neumann and
fully decoupled schemes for the coupling of
incompressible fluid with thin-walled structure

Yiyi HUANG (yhuangcm@connect.ust.hk, Dept. of Math, HKUST)

May 24, 2022

Contents

Table of Contents	2
List of Figures	3
List of Tables	4
Abstract	5
1 Introduction	1
2 The simplified model problem	2
3 Notations	4
4 Fernandez's Explicit Robin-Neumann and fully decoupled schemes	4
5 Two schemes with added force	6
6 A fully decoupled scheme based on Van Kan's projection method and with added force	8
7 Numerical experiments	10
8 Conclusions from numerical results	20
8.1 Conclusions for Algorithm 1 from Table 1	20
8.2 Conclusions for Algorithm 2 from Table 2	21
8.3 Conclusions for Algorithm 3 from Table 3	21
9 A possible and non-rigorous explanation for the behaviour of stability	22
10 Selection of β, θ and ξ for practical applications	22
11 Discussions and future work	26
12 Acknowledgments	27

List of Figures

1	Geometrial configuration	3
2	Structure displacement of Fernandez Explicit Robin-Neumann scheme (Fern ERN) and Algorithm 1 (Algo 1) with $\beta = 43$ at final time	26
3	Structure displacement of Fernandez fully decoupled scheme (Fern FD) and Algorithm 2 (Algo 2) with $\theta = 25$ at final time	27
4	Structure displacement of Fernandez fully decoupled scheme (Fern FD) and Algorithm 3 (Algo 3) with $\xi = 31$ at final time	28
5	Structure displacement of Fernandez fully decoupled scheme (Fern FD) and Algorithm 3 (Algo 3) with $\xi = 32$ at final time	29
6	Structure displacement of Fernandez fully decoupled scheme (Fern FD) and Algorithm 3 (Algo 3) with $\xi = 33$ at final time	30

List of Tables

1	Numerical results of Fernandez Explicit Robin-Neumann scheme (Fern ERN) and Algorithm 1 (Algo 1)	12
2	Numerical results of Fernandez fully decoupled scheme (Fern FD) and Algorithm 2 (Algo 2)	15
3	Numerical results of Fernandez fully decoupled scheme (Fern FD) and Algorithm 3 (Algo 3)	18
4	Numerical results of Fernandez Explicit Robin-Neumann scheme (Fern ERN) and Algorithm 1 (Algo 1) at selected β	23
5	Numerical results of Fernandez fully decoupled scheme (Fern FD) and Algorithm 2 (Algo 2) at selected θ	23
6	Numerical results of Fernandez fully decoupled scheme (Fern FD) and Algorithm 3 (Algo 3) at selected ξ	25

Abstract

Enlightened by added-mass effect and viscosity of fluid, in Explicit Robin-Neumann and fully decoupled schemes for the coupling of incompressible fluid with thin-walled structure, the force between fluid and structure corresponding to viscosity is increased. Numerical experiments demonstrate improvement of accuracy under such modification. To further improve accuracy of fully decoupled schemes, the underlying projection method is replaced.

1 Introduction

The coupling of incompressible fluid with thin-walled structure typically arises in subjects like bio-mechanics of blood flow in vessels [10], for which the blood is governed by Navier-Stokes equations, while the structure assumed to be deformable. Generally, like the numerical methods to other fluid-structure interaction problems, there are two types of numerical approaches, namely the monolithic (also named *fully implicit*) and partitioned (also named *decoupled*) [14]. The monolithic is accurate but less efficient, while the partitioned is much more efficient but not that accurate.

Among various partitioned algorithms on this topic [10, 14, 9, 6, 8, 7, 12, 3], Fernandez's **Explicit Robin-Neumann** [9] and **fully decoupled schemes** [6] [8] are exceptional, due to their high efficiency, theoretical and/or numerical stability and applicability to the topic with a vast variety of structure models. The **fully decoupled scheme** is more efficient than Explicit Robin-Neumann scheme, because the velocity and pressure of fluid are decoupled.

The infamous added-mass effect is known to cause instability to tremendous partitioned algorithms for fluid-structure interaction problems with large fluid/structure density ratio (for many problems the density of fluid is lower than that of structure, so this implies the density of fluid is large enough to be close to that of structure) and long thin geometry [18].

Intuitively, due to viscosity of fluid, when the fluid or structure moves, some amount of fluid is attached to it near the interface, resulting in "added" mass. By Newton's Second Law, the mass together with acceleration results in extra force on the structure. By Newton's Third Law, there is an equal and opposite force on the fluid. Thus, it is reasonable to expect, for a partitioned algorithm, increasing the force due to viscosity of fluid between the fluid and structure can make it more realistic, namely more close to the actual behaviour of the coupling system, which might lead to better accuracy. The amount of extra force resulting from "added" mass is difficult (if not impossible) to compute; however, it can be approached. Up to certain values, increasing the force gradually should improve accuracy gradually.

The idea is applied to Fernandez's two schemes mentioned above. Note that, however, this does not mean the two schemes are unstable; in fact, their stabilities have proved by theoretical analysis and/or numerical experiments (availability of theoretical analysis depends

on extrapolation orders) to be free of added-mass effect. In what follows, the two schemes are presented. Afterwards, coefficients of the terms corresponding to force from viscosity are increased, generating **Algorithm 1** and **Algorithm 2**. Fernandez’s **fully decoupled scheme** is based on Chorin-Temam projection method. To further improve accuracy, the underlying projection method is replaced with Van Kan’s, leading to **Algorithm 3**.

Numerical results are reported later. The results indicate improvement of accuracy as the force from viscosity increases. Appropriate values for such increment are recommended for practical applications.

Remark 1 Based on the intuition mentioned above, it might not be difficult to understand the reasons why added-mass effect causes instability to tremendous partitioned algorithms for fluid-structure interaction problems with large fluid/structure density ratio and long thin geometry. As the density of fluid increases, the part of fluid attached to the structure due to viscosity influences more seriously on the movement of structure. If the geometry is long and thin, such a part of fluid takes large portion of the whole fluid, which influences seriously on the movement of fluid. If it decouples the fluid and structure without paying sufficient attention to such effect, a partitioned algorithm might be far from the actual movement of the coupling system and thus might fail to finish the simulation, which constitutes stability issues.

2 The simplified model problem

For sake of clarity and simplicity, the simplified test-case used in [5] is adopted. This work is expected to be also applicable to the a bit more general model described in [9] [6] [8]. The fluid dominated by Stokes equations is defined on $\Omega = [0, L] \times [0, R]$, where $L = 6, R = 0.5$ (all the quantities are under CGS system) , with $\partial\Omega = \Gamma_1 \cup \Gamma_2 \cup \Sigma \cup \Gamma_4$ (see Figure 1) . The domain is extracted as upper half of the rectangle $[0, L] \times [-R, R]$ which simulates a tube in two-dimensional space with horizontal centerline Γ_1 and top boundary Σ . As a result, Γ_1 is imposed symmetric boundary condition. The structure is assumed to be a generalized string defined on Σ with the two end points ($x = 0, L$) fixed. When the fluid flows from the left to the right, structure deforms vertically. Equations read as follows.

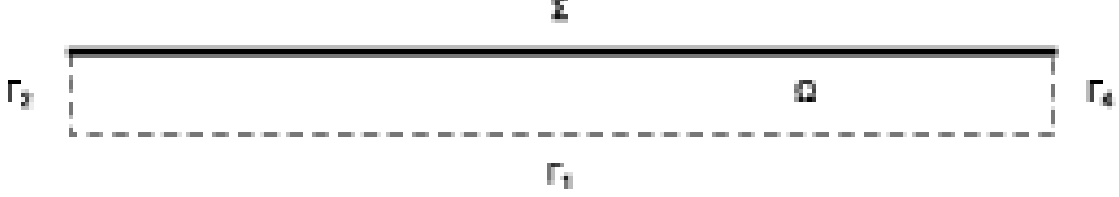


Figure 1: Geometrical configuration

Find the fluid velocity $\mathbf{u} : \Omega \times \mathbb{R}^+ \rightarrow \mathbb{R}^2$, the fluid pressure $p : \Omega \times \mathbb{R}^+ \rightarrow \mathbb{R}$, the structure vertical displacement $\eta : \Sigma \times \mathbb{R}^+ \rightarrow \mathbb{R}$ and the structure vertical velocity $\dot{\eta} : \Sigma \times \mathbb{R}^+ \rightarrow \mathbb{R}$ such that

$$\left\{ \begin{array}{ll} \rho^f \partial_t \mathbf{u} - \mathbf{div} \, \boldsymbol{\sigma}(\mathbf{u}, p) = \mathbf{0} & \text{in } \Omega, \\ \mathbf{div} \, \mathbf{u} = 0 & \text{in } \Omega, \\ \mathbf{u} \cdot \mathbf{n} = 0, \boldsymbol{\sigma}(\mathbf{u}, p) \mathbf{n} \cdot \mathbf{t} = 0 & \text{on } \Gamma_1, \\ \boldsymbol{\sigma}(\mathbf{u}, p) \mathbf{n} = -P(t) \mathbf{n} & \text{on } \Gamma_2, \\ \boldsymbol{\sigma}(\mathbf{u}, p) \mathbf{n} = \mathbf{0} & \text{on } \Gamma_4, \end{array} \right. \quad (1)$$

$$\left\{ \begin{array}{ll} \mathbf{u} \cdot \mathbf{n} = \dot{\eta}, \mathbf{u} \cdot \mathbf{t} = 0 & \text{on } \Sigma, \\ \rho^s \epsilon \partial_t \dot{\eta} - c_1 \partial_{xx} \eta + c_0 \eta = -\boldsymbol{\sigma}(\mathbf{u}, p) \mathbf{n} \cdot \mathbf{n} & \text{on } \Sigma, \\ \dot{\eta} = \partial_t \eta & \text{on } \Sigma, \\ \eta = 0 & \text{on } \partial \Sigma, \end{array} \right. \quad (2)$$

with initial conditions

$$\mathbf{u}(0) = \mathbf{0}, \eta(0) = 0, \dot{\eta}(0) = 0,$$

where normal vector is denoted by \mathbf{n} , tangent vector is \mathbf{t} , fluid Cauchy stress tensor $\boldsymbol{\sigma}(\mathbf{u}, p) \stackrel{\text{def}}{=} -p\mathbf{I} + 2\mu\boldsymbol{\varepsilon}(\mathbf{u})$, $\boldsymbol{\varepsilon}(\mathbf{u}) \stackrel{\text{def}}{=} \frac{1}{2}(\nabla \mathbf{u} + \nabla \mathbf{u}^T)$, fluid dynamic viscosity $\mu = 0.035$, fluid density $\rho^f = 1.0$, pressure $P(t) = P_{max}(1 - \cos(2t\pi/T^*))/2$, $P_{max} = 2 * 10^4$ when $0 \leq t \leq T^*$ and $P_{max} = 0$ when $t > T^*$, $T^* = 5 * 10^{-3}$, structure density $\rho^s = 1.1$, $c_1 \stackrel{\text{def}}{=} \frac{E\epsilon}{2(1+\nu)}$, $c_0 \stackrel{\text{def}}{=} \frac{E\epsilon}{R^2(1-\nu^2)}$, $\epsilon = 0.1$, Young's modulus $E = 0.75 * 10^6$, Poisson's ratio $\nu = 0.5$.

3 Notations

For all the algorithms mentioned in this work, τ denotes time step, while h stands for space discretization parameter.

Given arbitrary variable x , the notation

$$x^{n,\star} \stackrel{\text{def}}{=} \begin{cases} 0 & \text{if } r = 0, \\ x^{n-1} & \text{if } r = 1, \\ 2x^{n-1} - x^{n-2} & \text{if } r = 2 \end{cases} \quad (3)$$

is used for interface extrapolations of order r .

4 Fernandez's Explicit Robin-Neumann and fully decoupled schemes

The time semi-discrete form of **Explicit Robin-Neumann scheme** (Fernandez [9]) is cited here.

(Fernandez) Explicit Robin-Neumann scheme (time semi-discrete)

For $n \geq r + 1$, find $\mathbf{u}^n : \Omega \rightarrow \mathbb{R}^2$, $p^n : \Omega \rightarrow \mathbb{R}$, $\eta^n : \Sigma \rightarrow \mathbb{R}$ and $\dot{\eta}^n : \Sigma \rightarrow \mathbb{R}$ such that

1. Fluid step (interface Robin condition)

$$\left\{ \begin{array}{ll} \rho^f \frac{\mathbf{u}^n - \mathbf{u}^{n-1}}{\tau} \mathbf{u}^n - \mathbf{div} \, \boldsymbol{\sigma}(\mathbf{u}^n, p^n) = \mathbf{0} & \text{in } \Omega, \\ \mathbf{div} \, \mathbf{u}^n = 0 & \text{in } \Omega, \\ \mathbf{u}^n \cdot \mathbf{n} = 0, \boldsymbol{\sigma}(\mathbf{u}^n, p^n) \mathbf{n} \cdot \mathbf{t} = 0 & \text{on } \Gamma_1, \\ \boldsymbol{\sigma}(\mathbf{u}^n, p^n) \mathbf{n} = -P(t) \mathbf{n} & \text{on } \Gamma_2, \\ \boldsymbol{\sigma}(\mathbf{u}^n, p^n) \mathbf{n} = \mathbf{0} & \text{on } \Gamma_4, \\ \boldsymbol{\sigma}(\mathbf{u}^n, p^n) \mathbf{n} \cdot \mathbf{n} + \frac{\rho^s \epsilon}{\tau} \mathbf{u}^n \cdot \mathbf{n} = \frac{\rho^s \epsilon}{\tau} (\dot{\eta}^{n-1} + \tau \partial_\tau \dot{\eta}^{n,\star}) \\ \quad + (-p^{n,\star} \mathbf{I} + 2\mu \boldsymbol{\varepsilon}(\mathbf{u}^{n,\star})) \mathbf{n} \cdot \mathbf{n} & \text{on } \Sigma, \\ \mathbf{u}^n \cdot \mathbf{t} = 0 & \text{on } \Sigma. \end{array} \right. \quad (4)$$

2. Solid step (Neumann condition)

$$\left\{ \begin{array}{ll} \rho^s \epsilon \frac{\dot{\eta}^n - \dot{\eta}^{n-1}}{\tau} - c_1 \partial_{xx} \eta^n + c_0 \eta^n = -(-p^n \mathbf{I} + 2\mu \boldsymbol{\varepsilon}(\mathbf{u}^n)) \mathbf{n} \cdot \mathbf{n} & \text{on } \Sigma, \\ \dot{\eta}^n = \partial_\tau \eta^n & \text{on } \Sigma, \\ \eta^n = 0 & \text{on } \partial\Sigma, \end{array} \right. \quad (5)$$

The **fully decoupled scheme** is proposed in Fernandez [6], [8]. There are non-incremental and incremental forms, of which both deliver close numerical results on accuracy. Here only presents the non-incremental form.

(Fernandez) fully decoupled scheme (time semi-discrete)

For $n \geq r + 1$,

(1) Fluid viscous sub-step: find $\tilde{\mathbf{u}}^n : \Omega \rightarrow \mathbb{R}^2$ such that

$$\left\{ \begin{array}{ll} \rho^f \frac{\tilde{\mathbf{u}}^n - \mathbf{u}^{n-1}}{\tau} - 2\mu \operatorname{div} \boldsymbol{\varepsilon}(\tilde{\mathbf{u}}^n) = 0 & \text{in } \Omega, \\ \tilde{\mathbf{u}}^n \cdot \mathbf{n} = 0, 2\mu \boldsymbol{\varepsilon}(\tilde{\mathbf{u}}^n) \mathbf{n} \cdot \boldsymbol{\tau} = 0 & \text{on } \Gamma_1, \\ 2\mu \boldsymbol{\varepsilon}(\tilde{\mathbf{u}}^n) \mathbf{n} \cdot \boldsymbol{\tau} = 0 & \text{on } \Gamma_2, \\ 2\mu \boldsymbol{\varepsilon}(\tilde{\mathbf{u}}^n) \mathbf{n} \cdot \boldsymbol{\tau} = 0 & \text{on } \Gamma_4, \\ \tilde{u}_1^n = 0, 2\mu \boldsymbol{\varepsilon}(\tilde{\mathbf{u}}^n) \mathbf{n} \cdot \mathbf{n} + \frac{\rho^s \epsilon}{\tau} \tilde{\mathbf{u}}^n \cdot \mathbf{n} = \frac{\rho^s \epsilon}{\tau} \dot{\eta}^{n-1} & \text{on } \Sigma, \end{array} \right. \quad (6)$$

(2) Fluid projection sub-step: find $\phi^n : \Omega \rightarrow \mathbb{R}^2$ such that

$$\left\{ \begin{array}{ll} -\frac{\tau}{\rho^f} \Delta \phi^n = -\nabla \cdot \tilde{\mathbf{u}}^n & \text{in } \Omega, \\ \frac{\partial \phi^n}{\partial n} = 0 & \text{on } \Gamma_1, \\ \phi^n = P(t_n) & \text{on } \Gamma_2, \\ \phi^n = 0 & \text{on } \Gamma_4, \\ \frac{\tau}{\rho^f} \nabla \phi^n \cdot \mathbf{n} + \frac{\tau}{\rho^s \epsilon} \phi^n = \frac{\tau}{\rho^s \epsilon} \phi^{n,*} + \tilde{\mathbf{u}}^{n,*} \cdot \mathbf{n} - \dot{\eta}^{n,*} & \text{on } \Sigma, \end{array} \right. \quad (7)$$

Thereafter set $p^n = \phi^n$, $\mathbf{u}^n = \tilde{\mathbf{u}}^n - \frac{\tau}{\rho^f} \nabla \phi^n$ in Ω .

(3) Solid sub-step: find $\eta^n : \Sigma \rightarrow \mathbb{R}^2$ such that

$$\left\{ \begin{array}{ll} \rho^s \epsilon \frac{\dot{\eta}^n - \dot{\eta}^{n-1}}{\tau} - c_1 \partial_{xx} \eta^n + c_0 \eta^n = -2\mu \boldsymbol{\varepsilon}(\tilde{\mathbf{u}}^n) \mathbf{n} \cdot \mathbf{n} + p^n & \text{on } \Sigma, \\ \dot{\eta}^n = \frac{\eta^n - \eta^{n-1}}{\tau} & \text{on } \Sigma, \\ \eta^n = 0 & \text{on } \partial\Sigma, \end{array} \right. \quad (8)$$

Remark 2 Substituting $\mathbf{u}^n = \tilde{\mathbf{u}}^n - \frac{\tau}{\rho^f} \nabla \phi^n$ into (6)₁ leads to a more compact style, with \mathbf{u}^n eliminated (see [6]).

5 Two schemes with added force

Replacing the coefficient 2 in the term $2\mu \boldsymbol{\varepsilon}(\mathbf{u}^{n,*})$ at the right hand side of (4)₆ and the term $2\mu \boldsymbol{\varepsilon}(\mathbf{u}^n)$ at the right hand side of (5)₁ with a real number named β larger than 2 generates **Algorithm 1** as follows. Analogously, substituting the coefficient 2 in the term $-2\mu \boldsymbol{\varepsilon}(\tilde{\mathbf{u}}^n) \mathbf{n} \cdot \mathbf{n}$ at the right hand side of (8)₁ with a real number named θ larger than 2 leads to **Algorithm 2**.

Remark 3 There is no such a term in (6)₅ like $(-p^{n,*} \mathbf{I} + 2\mu \boldsymbol{\varepsilon}(\mathbf{u}^{n,*})) \mathbf{n} \cdot \mathbf{n}$ of (4)₆, so there is no such a term in (11)₅ like $(-p^{n,*} \mathbf{I} + \beta \mu \boldsymbol{\varepsilon}(\mathbf{u}^{n,*})) \mathbf{n} \cdot \mathbf{n}$ of (9)₆

Algorithm 1

For real number $\beta > 2, n \geq r+1$, find $\mathbf{u}^n : \Omega \rightarrow \mathbb{R}^2, p^n : \Omega \rightarrow \mathbb{R}, \eta^n : \Sigma \rightarrow \mathbb{R}$ and $\dot{\eta}^n : \Sigma \rightarrow \mathbb{R}$ such that

1. Fluid step (interface Robin condition)

$$\left\{ \begin{array}{llll} \rho^f \frac{\mathbf{u}^n - \mathbf{u}^{n-1}}{\tau} - \mathbf{div} \, \boldsymbol{\sigma}(\mathbf{u}^n, p^n) = \mathbf{0} & \text{in} & \Omega, \\ \mathbf{div} \, \mathbf{u}^n = 0 & \text{in} & \Omega, \\ \mathbf{u}^n \cdot \mathbf{n} = 0, \boldsymbol{\sigma}(\mathbf{u}^n, p^n) \mathbf{n} \cdot \mathbf{t} = 0 & \text{on} & \Gamma_1, \\ \boldsymbol{\sigma}(\mathbf{u}^n, p^n) \mathbf{n} = -P(t) \mathbf{n} & \text{on} & \Gamma_2, \\ \boldsymbol{\sigma}(\mathbf{u}^n, p^n) \mathbf{n} = \mathbf{0} & \text{on} & \Gamma_4, \\ \boldsymbol{\sigma}(\mathbf{u}^n, p^n) \mathbf{n} \cdot \mathbf{n} + \frac{\rho^s \epsilon}{\tau} \mathbf{u}^n \cdot \mathbf{n} = \frac{\rho^s \epsilon}{\tau} (\dot{\eta}^{n-1} + \tau \partial_\tau \dot{\eta}^{n,*}) \\ \quad + (-p^{n,*} \mathbf{I} + \beta \mu \boldsymbol{\varepsilon}(\mathbf{u}^{n,*})) \mathbf{n} \cdot \mathbf{n} & \text{on} & \Sigma, \\ \mathbf{u}^n \cdot \mathbf{t} = 0 & \text{on} & \Sigma. \end{array} \right. \quad (9)$$

2. Solid step (Neumann condition)

$$\left\{ \begin{array}{llll} \rho^s \epsilon \frac{\dot{\eta}^n - \dot{\eta}^{n-1}}{\tau} - c_1 \partial_{xx} \eta^n + c_0 \eta^n = -(-p^n \mathbf{I} + \beta \mu \boldsymbol{\varepsilon}(\mathbf{u}^n)) \mathbf{n} \cdot \mathbf{n} & \text{on} & \Sigma, \\ \dot{\eta}^n = \partial_\tau \eta^n & \text{on} & \Sigma, \\ \eta^n = 0 & \text{on} & \partial \Sigma, \end{array} \right. \quad (10)$$

Algorithm 2

For real number $\theta > 2$, $n \geq r + 1$,

(1) Fluid viscous sub-step: find $\tilde{\mathbf{u}}^n : \Omega \rightarrow \mathbb{R}^2$ such that

$$\left\{ \begin{array}{llll} \rho^f \frac{\tilde{\mathbf{u}}^n - \mathbf{u}^{n-1}}{\tau} - 2\mu \mathbf{div} \, \boldsymbol{\varepsilon}(\tilde{\mathbf{u}}^n) = \mathbf{0} & \text{in} & \Omega, \\ \tilde{\mathbf{u}}^n \cdot \mathbf{n} = 0, 2\mu \boldsymbol{\varepsilon}(\tilde{\mathbf{u}}^n) \mathbf{n} \cdot \boldsymbol{\tau} = 0 & \text{on} & \Gamma_1, \\ 2\mu \boldsymbol{\varepsilon}(\tilde{\mathbf{u}}^n) \mathbf{n} \cdot \boldsymbol{\tau} = 0 & \text{on} & \Gamma_2, \\ 2\mu \boldsymbol{\varepsilon}(\tilde{\mathbf{u}}^n) \mathbf{n} \cdot \boldsymbol{\tau} = 0 & \text{on} & \Gamma_4, \\ \tilde{u}_1^n = 0, 2\mu \boldsymbol{\varepsilon}(\tilde{\mathbf{u}}^n) \mathbf{n} \cdot \mathbf{n} + \frac{\rho^s \epsilon}{\tau} \tilde{\mathbf{u}}^n \cdot \mathbf{n} = \frac{\rho^s \epsilon}{\tau} \dot{\eta}^{n-1} & \text{on} & \Sigma, \end{array} \right. \quad (11)$$

(2) Fluid projection sub-step: find $\phi^n : \Omega \rightarrow \mathbb{R}^2$ such that

$$\left\{ \begin{array}{ll} -\frac{\tau}{\rho^f} \Delta \phi^n = -\nabla \cdot \tilde{\mathbf{u}}^n & \text{in } \Omega, \\ \frac{\partial \phi^n}{\partial n} = 0 & \text{on } \Gamma_1, \\ \phi^n = P(t_n) & \text{on } \Gamma_2, \\ \phi^n = 0 & \text{on } \Gamma_4, \\ \frac{\tau}{\rho^f} \nabla \phi^n \cdot \mathbf{n} + \frac{\tau}{\rho^s \epsilon} \phi^n = \frac{\tau}{\rho^s \epsilon} \phi^{n,*} + \tilde{\mathbf{u}}^{n,*} \cdot \mathbf{n} - \dot{\eta}^{n,*} & \text{on } \Sigma, \end{array} \right. \quad (12)$$

Thereafter set $p^n = \phi^n$, $\mathbf{u}^n = \tilde{\mathbf{u}}^n - \frac{\tau}{\rho^f} \nabla \phi^n$ in Ω .

(3) Solid sub-step: find $\eta^n : \Sigma \rightarrow \mathbb{R}^2$ such that

$$\left\{ \begin{array}{ll} \rho^s \epsilon \frac{\dot{\eta}^n - \dot{\eta}^{n-1}}{\tau} - c_1 \partial_{xx} \eta^n + c_0 \eta^n = -\theta \mu \epsilon (\tilde{\mathbf{u}}^n) \mathbf{n} \cdot \mathbf{n} + p^n & \text{on } \Sigma, \\ \dot{\eta}^n = \frac{\eta^n - \eta^{n-1}}{\tau} & \text{on } \Sigma, \\ \eta^n = 0 & \text{on } \partial \Sigma, \end{array} \right. \quad (13)$$

6 A fully decoupled scheme based on Van Kan's projection method and with added force

Fernandez's **fully decoupled scheme** is based on Chorin-Temam projection method, whose accuracy is of first order in time (see e.g. [16] [13]). It is expected, if the underlying projection method is replaced with Van Kan's projection method, which is of second order in time (see e.g. [16]), such schemes could be more accurate. This idea produces **Algorithms 3**.

Algorithm 3

For real number $\xi \geq 2$, $n \geq r + 1$,

(1) Fluid viscous sub-step: find $\tilde{\mathbf{u}}^n : \Omega \rightarrow \mathbb{R}^2$ such that

$$\left\{ \begin{array}{ll} \rho^f \frac{\tilde{\mathbf{u}}^n - \mathbf{u}^{n-1}}{\tau} = -\nabla p^{n-1} + \frac{1}{2}(2\mu \operatorname{div} \varepsilon(\tilde{\mathbf{u}}^n) + 2\mu \operatorname{div} \varepsilon(\mathbf{u}^{n-1})) & \text{in } \Omega, \\ \tilde{\mathbf{u}}^n \cdot \mathbf{n} = 0, 2\mu \varepsilon(\tilde{\mathbf{u}}^n) \mathbf{n} \cdot \boldsymbol{\tau} = 0 & \text{on } \Gamma_1, \\ 2\mu \varepsilon(\tilde{\mathbf{u}}^n) \mathbf{n} \cdot \boldsymbol{\tau} = 0 & \text{on } \Gamma_2, \\ 2\mu \varepsilon(\tilde{\mathbf{u}}^n) \mathbf{n} \cdot \boldsymbol{\tau} = 0 & \text{on } \Gamma_4, \\ \tilde{u}_1^n = 0, 2\mu \varepsilon(\tilde{\mathbf{u}}^n) \mathbf{n} \cdot \mathbf{n} + \frac{\rho^s \epsilon}{\tau} \tilde{\mathbf{u}}^n \cdot \mathbf{n} = \frac{\rho^s \epsilon}{\tau} \dot{\eta}^{n-1} & \text{on } \Sigma, \end{array} \right. \quad (14)$$

(2) Fluid projection sub-step: find $\phi^n : \Omega \rightarrow \mathbb{R}^2$ such that

$$\left\{ \begin{array}{ll} -\frac{\tau}{\rho^f} \Delta \phi^n = -\nabla \cdot \tilde{\mathbf{u}}^n & \text{in } \Omega, \\ \frac{\partial \phi^n}{\partial n} = 0 & \text{on } \Gamma_1, \\ \phi^n = \frac{P(t_n) - P(t_{n-1})}{2} & \text{on } \Gamma_2, \\ \phi^n = 0 & \text{on } \Gamma_4, \\ \frac{\tau}{\rho^f} \nabla \phi^n \cdot \mathbf{n} + \frac{\tau}{\rho^s \epsilon} \phi^n = \\ \frac{\tau}{\rho^s \epsilon} \frac{p^{n,\star} - p^{n-1,\star}}{2} + \frac{\tilde{\mathbf{u}}^{n,\star} - \tilde{\mathbf{u}}^{n-1,\star}}{2} \cdot \mathbf{n} - \frac{\dot{\eta}^{n,\star} - \dot{\eta}^{n-1,\star}}{2} & \text{on } \Sigma, \end{array} \right. \quad (15)$$

Thereafter set $p^n = p^{n-1} + 2\phi^n$, $\mathbf{u}^n = \tilde{\mathbf{u}}^n - \frac{\tau}{\rho^f} \nabla \phi^n$ in Ω .

(3) Solid sub-step: find $\eta^n : \Sigma \rightarrow \mathbb{R}^2$ such that

$$\left\{ \begin{array}{ll} \rho^s \epsilon \frac{\dot{\eta}^n - \dot{\eta}^{n-1}}{\tau} - c_1 \partial_{xx} \eta^n + c_0 \eta^n = -\xi \mu \varepsilon(\tilde{\mathbf{u}}^n) \mathbf{n} \cdot \mathbf{n} + p^n & \text{on } \Sigma, \\ \dot{\eta}^n = \frac{\eta^n - \eta^{n-1}}{\tau} & \text{on } \Sigma, \\ \eta^n = 0 & \text{on } \partial \Sigma, \end{array} \right. \quad (16)$$

Remark 4 Boundary conditions for the fluid projection sub-step of **Algorithm 3** are deduced from that of **Fernandez's fully decoupled scheme** by noting that $\phi^n = \frac{p^n - p^{n-1}}{2}$ for **Algorithm 3** and that $p^n = \phi^n$ for **Fernandez's fully decoupled scheme**. For example, on Γ_2 , (7)₃ indicates

$$\begin{aligned} p^n &= P(t_n) \\ p^{n-1} &= P(t_{n-1}) \end{aligned}$$

Taking the difference and divided by 2 yields (15)₃

$$\phi^n = \frac{p^n - p^{n-1}}{2} = \frac{P(t_n) - P(t_{n-1})}{2}$$

The same procedure applies to the deduction of (15)_{2,4,5}

7 Numerical experiments

Fernandez's two algorithms and **Algorithms 1-3** are all discretized with Galerkin finite element method in space and implemented with FreeFem++ [15] using Lagrange P_1 element for both the fluid and structure with symmetric pressure stabilization method [2]. In order to observe the order of convergence, the time and space are refined at the same *rate*,

$$(\tau, h) = \frac{(5 * 10^{-4}, 0.1)}{2^{rate}}, \quad rate = 0, 1, 2, 3, 4, 5, \dots$$

The reference solution is generated using monolithic scheme at high time-space grid resolution $\tau = 10^{-6}$, $h = 3.125 \times 10^{-3}$. All algorithms run from initial time $t = 0$ to final time $t = 0.015$. By comparing solutions of the above 5 schemes to reference solution, relative errors in elastic energy norm (see [9]) are computed for structure displacement at final time corresponding to different *rates* of space and time refinement.

Computation of relative errors and preparation of data for writing are completed with Perl [20] as well as an amount of Perl modules [17] and Bash [11]. Graphs are drew using gnuplot [21]. All codes run on x86_64 Linux 5.6.0 [19] with one Intel[®] Xeon[®] E-2186M CPU @ 2.90GHz.

Tables 1, 2 and 3 report relative errors of Fernandez's two algorithms and **Algorithms 1-3** with β, θ and ξ ranging from integers 10 to 45 respectively, at refinement *rate* = 2, 3, 4, 5. The refinement *rate* = 0 and 1 are of no interest and not presented, since all of Fernandez's two algorithms and **Algorithms 1-3** perform poorly in accuracy at such low *rates*. Numerical results of **Algorithms 1-3** with β, θ and ξ ranging from 2 to 10 are not presented, because they do not yield obvious improvement of accuracy at these intervals.

Both of Fernandez's two algorithms achieve both highest accuracy and optimal first-order convergence rate in time with first-order extrapolation, so Tables 1, 2 and 3 include

their results at first-order extrapolation only. For purpose of comparison, **Algorithm 1** and **2** are also computed with first-order extrapolation. However, **Algorithm 3** reaches highest accuracy at zeroth-order extrapolation, so its results at zeroth-order extrapolation are presented.

Table 1: Numerical results of Fernandez Explicit Robin-Neumann scheme (Fern ERN) and Algorithm 1 (Algo 1)

rate	Fern ERN	Algo 1 $\beta = 10$	Algo 1 $\beta = 11$	Algo 1 $\beta = 12$	Algo 1 $\beta = 13$	Algo 1 $\beta = 14$
2	0.435176	0.423118	0.421689	0.420281	0.418895	0.417532
3	0.241766	0.233158	0.232109	0.231066	0.230030	0.229001
4	0.128616	0.123319	0.122668	0.122021	0.121377	0.120735
5	0.064847	0.061810	0.061437	0.061066	0.060696	0.060328

rate	Algo 1 $\beta = 15$	Algo 1 $\beta = 16$	Algo 1 $\beta = 17$	Algo 1 $\beta = 18$	Algo 1 $\beta = 19$	Algo 1 $\beta = 20$
2	0.416193	0.414879	0.413592	0.412334	0.411104	0.409906
3	0.227979	0.226965	0.225959	0.224962	0.223972	0.222992
4	0.120097	0.119462	0.118831	0.118202	0.117578	0.116957
5	0.059961	0.059597	0.059234	0.058873	0.058514	0.058156

rate	Algo 1 $\beta = 21$	Algo 1 $\beta = 22$	Algo 1 $\beta = 23$	Algo 1 $\beta = 24$	Algo 1 $\beta = 25$	Algo 1 $\beta = 26$
2	0.408739	0.407606	0.406510	0.405836	unstable	unstable
3	0.222021	0.221059	0.220107	0.219165	0.218234	0.217313
4	0.116340	0.115727	0.115117	0.114512	0.113911	0.113314
5	0.057802	0.057449	0.057097	0.056748	0.056402	0.056057

rate	Algo 1	Algo 1	Algo 1	Algo 1	Algo 1	Algo 1
	$\beta = 27$	$\beta = 28$	$\beta = 29$	$\beta = 30$	$\beta = 31$	$\beta = 32$
2	unstable	unstable	unstable	unstable	unstable	unstable
3	0.216403	0.215505	0.214619	0.213744	0.212883	0.212034
4	0.112722	0.112134	0.111551	0.110973	0.110399	0.109831
5	0.055715	0.055375	0.055038	0.054703	0.054371	0.054041

rate	Algo 1	Algo 1	Algo 1	Algo 1	Algo 1	Algo 1
	$\beta = 33$	$\beta = 34$	$\beta = 35$	$\beta = 36$	$\beta = 37$	$\beta = 38$
2	unstable	unstable	unstable	unstable	unstable	unstable
3	0.211198	0.210376	0.209568	0.208775	0.207996	0.207233
4	0.109268	0.108710	0.108157	0.107610	0.107069	0.106536
5	0.053714	0.053389	0.053068	0.052749	0.052433	0.052121

rate	Algo 1	Algo 1	Algo 1	Algo 1	Algo 1	Algo 1
	$\beta = 39$	$\beta = 40$	$\beta = 41$	$\beta = 42$	$\beta = 43$	$\beta = 44$
2	unstable	unstable	unstable	unstable	unstable	unstable
3	0.206485	0.205754	0.205038	0.204341	0.203850	unstable
4	0.106004	0.105481	0.104966	0.104455	0.103949	0.103452
5	0.051811	0.051504	0.051201	0.050901	0.050604	0.050310

rate	Algo 1
	$\beta = 45$
2	unstable
3	unstable
4	0.102961
5	0.050021

Table 2: Numerical results of Fernandez fully decoupled scheme (Fern FD) and Algorithm 2 (Algo 2)

rate	Fern FD	Algo 2 $\theta = 10$	Algo 2 $\theta = 11$	Algo 2 $\theta = 12$	Algo 2 $\theta = 13$	Algo 2 $\theta = 14$
2	0.437713	0.420421	0.418264	0.416110	0.413961	0.411817
3	0.243562	0.231346	0.229813	0.228279	0.226744	0.225208
4	0.129731	0.123637	0.122873	0.122109	0.121345	0.120580
5	0.065497	0.063052	0.062746	0.062441	0.062136	0.061830

rate	Algo 2 $\theta = 15$	Algo 2 $\theta = 16$	Algo 2 $\theta = 17$	Algo 2 $\theta = 18$	Algo 2 $\theta = 19$	Algo 2 $\theta = 20$
2	0.409654	unstable	unstable	unstable	unstable	unstable
3	0.223672	0.222135	0.220599	0.219063	0.217527	0.215992
4	0.119816	0.119050	0.118285	0.117519	0.116754	0.115988
5	0.061525	0.061220	0.060915	0.060610	0.060305	0.060000

rate	Algo 2 $\theta = 21$	Algo 2 $\theta = 22$	Algo 2 $\theta = 23$	Algo 2 $\theta = 24$	Algo 2 $\theta = 25$	Algo 2 $\theta = 26$
2	unstable	unstable	unstable	unstable	unstable	unstable
3	0.214458	0.212924	0.211393	0.209862	0.208879	unstable
4	0.115222	0.114456	0.113690	0.112924	0.112158	0.111392
5	0.059695	0.059391	0.059086	0.058782	0.058477	0.058173

rate	Algo 2 $\theta = 27$	Algo 2 $\theta = 28$	Algo 2 $\theta = 29$	Algo 2 $\theta = 30$	Algo 2 $\theta = 31$	Algo 2 $\theta = 32$
2	unstable	unstable	unstable	unstable	unstable	unstable
3	unstable	unstable	unstable	unstable	unstable	unstable
4	0.110627	0.109861	0.109096	0.108330	0.107566	0.106801
5	0.057869	0.057565	0.057261	0.056958	0.056654	0.056351

rate	Algo 2 $\theta = 33$	Algo 2 $\theta = 34$	Algo 2 $\theta = 35$	Algo 2 $\theta = 36$	Algo 2 $\theta = 37$	Algo 2 $\theta = 38$
2	unstable	unstable	unstable	unstable	unstable	unstable
3	unstable	unstable	unstable	unstable	unstable	unstable
4	0.106036	0.105272	0.104509	0.103746	0.102984	0.102222
5	0.056048	0.055745	0.055442	0.055139	0.054837	0.054534

rate	Algo 2 $\theta = 39$	Algo 2 $\theta = 40$	Algo 2 $\theta = 41$	Algo 2 $\theta = 42$	Algo 2 $\theta = 43$	Algo 2 $\theta = 44$
2	unstable	unstable	unstable	unstable	unstable	unstable
3	unstable	unstable	unstable	unstable	unstable	unstable
4	0.101463	0.100700	0.099940	0.099186	unstable	unstable
5	0.054232	0.053931	0.053629	0.053327	0.053027	0.052726

rate	Algo 2
	$\theta = 45$
2	unstable
3	unstable
4	unstable
5	0.052425

Table 3: Numerical results of Fernandez fully decoupled scheme (Fern FD) and Algorithm 3 (Algo 3)

rate	Fern FD	Algo 3 $\xi = 10$	Algo 3 $\xi = 11$	Algo 3 $\xi = 12$	Algo 3 $\xi = 13$	Algo 3 $\xi = 14$
2	0.437713	0.413443	0.408376	0.403425	0.398606	0.393939
3	0.243562	0.248517	0.243651	0.238858	0.234148	0.229535
4	0.129731	0.136471	0.132807	0.129173	0.125574	0.122016
5	0.065497	0.069889	0.067621	0.065367	0.063132	0.060917

rate	Algo 3 $\xi = 15$	Algo 3 $\xi = 16$	Algo 3 $\xi = 17$	Algo 3 $\xi = 18$	Algo 3 $\xi = 19$	Algo 3 $\xi = 20$
2	0.389442	0.385136	0.381043	0.377186	0.373591	0.370281
3	0.225031	0.220650	0.216408	0.212321	0.208408	0.204686
4	0.118508	0.115057	0.111672	0.108363	0.105142	0.102021
5	0.058728	0.056566	0.054439	0.052351	0.050309	0.048320

rate	Algo 3 $\xi = 21$	Algo 3 $\xi = 22$	Algo 3 $\xi = 23$	Algo 3 $\xi = 24$	Algo 3 $\xi = 25$	Algo 3 $\xi = 26$
2	0.367286	0.364632	0.362348	0.360462	0.359005	0.358005
3	0.201178	0.197904	0.194886	0.192147	0.189712	0.187604
4	0.099015	0.096139	0.093410	0.090847	0.088472	0.086299
5	0.046394	0.044540	0.042769	0.041095	0.039531	0.038095

rate	Algo 3	Algo 3	Algo 3	Algo 3	Algo 3	Algo 3
	$\xi = 27$	$\xi = 28$	$\xi = 29$	$\xi = 30$	$\xi = 31$	$\xi = 32$
2	0.357492	0.357517	0.358058	0.359165	0.360862	0.363169
3	0.185846	0.184461	0.183471	0.182897	0.182757	0.183065
4	0.084358	0.082669	0.081254	0.080136	0.079329	0.078857
5	0.036802	0.035672	0.034723	0.033973	0.033437	0.033131

rate	Algo 3	Algo 3	Algo 3	Algo 3	Algo 3	Algo 3
	$\xi = 33$	$\xi = 34$	$\xi = 35$	$\xi = 36$	$\xi = 37$	$\xi = 38$
2	0.366107	0.369690	0.373933	0.378845	0.384418	0.392112
3	0.183835	0.185076	0.186796	0.188994	0.191672	0.194826
4	0.078730	0.078957	0.079543	0.080489	0.081789	0.083434
5	0.033061	0.033234	0.033648	0.034298	0.035172	0.036259

rate	Algo 3	Algo 3	Algo 3	Algo 3	Algo 3	Algo 3
	$\xi = 39$	$\xi = 40$	$\xi = 41$	$\xi = 42$	$\xi = 43$	$\xi = 44$
2	unstable	unstable	unstable	unstable	unstable	unstable
3	0.198449	0.202535	0.207070	0.212044	0.217443	0.223253
4	0.085413	0.087711	0.090310	0.093194	0.096343	0.099741
5	0.037542	0.039004	0.040630	0.042402	0.044305	0.046326

rate	Algo 3
	$\xi = 45$
2	unstable
3	0.229459
4	0.103370
5	0.048453

8 Conclusions from numerical results

Conclusions can be drawn from Tables 1, 2 and 3 respectively as follows.

8.1 Conclusions for Algorithm 1 from Table 1

Relative errors of **Algorithm 1** decrease in a regular manner as β or refinement *rate* increase. All the relative errors are less than that of **Fernandez Explicit Robin-Neumann scheme** except for unstable ones. All algorithms roughly achieve the same convergence order in time, namely $\mathcal{O}(t)$.

Stability is conditional. For a specific value of β , the algorithm is stable at high refinement *rates*; for a specific refinement *rate*, it is stable at small values of β . At *rate* = 2 and 3, **Algorithm 1** is stable up to $\beta = 24$ and 43 respectively. At *rate* = 4 and 5, it is stable for all tested values of β .

That relative errors keep decreasing as β increases up to 45 implies that the amount of force added to the algorithm keeps approaching the actual amount of force resulting from added-mass effect in the coupling system. Based on the intuition mentioned in **Section 1**, it is guessed continuing increasing β up to certain value larger than 45 might decrease the relative errors further. However, since the algorithm performs worse in stability at larger β and the stability is already frustrating at $\beta = 45$, it is not worth doing so.

8.2 Conclusions for Algorithm 2 from Table 2

Relative errors of **Algorithm 2** decrease in a regular manner as θ or refinement *rate* increase. All the relative errors are less than that of **Fernandez fully decoupled scheme** except for unstable ones. All algorithms roughly achieve the same convergence order in time, namely $\mathcal{O}(t)$.

Stability is conditional. For a specific value of θ , the algorithm is stable at high refinement *rates*; for a specific refinement *rate*, it is stable at small values of θ . At *rate* = 2, 3 and 4, **Algorithm 2** is stable up to $\theta = 15$, 25 and 42 respectively. At *rate* = 5, it is stable for all tested values of θ .

That relative errors keep decreasing as θ increases up to 45 implies that the amount of force added to the algorithm keeps approaching the actual amount of force resulting from added-mass effect in the coupling system. Based on the intuition mentioned in **Section 1**, it is guessed continuing increasing θ up to certain value larger than 45 might decrease the relative errors further. However, since the algorithm performs worse in stability at larger θ and the stability is already frustrating at $\theta = 45$, it is not worth doing so.

8.3 Conclusions for Algorithm 3 from Table 3

Relative errors of **Algorithm 3** decrease in a regular manner as ξ or refinement *rate* increase up to $\xi = 27$ at *rate* = 2, $\xi = 31$ at *rate* = 3, $\xi = 33$ at *rate* = 4 and $\xi = 33$ at *rate* = 5. For larger ξ at that refinement *rate*, relative errors augment. All the relative errors are less than that of **Fernandez fully decoupled scheme** except for unstable ones. All algorithms roughly achieve the same convergence order in time, namely $\mathcal{O}(t)$.

Stability is conditional. For a specific value of ξ , the algorithm is stable at high refinement *rates*; for a specific refinement *rate*, it is stable at small values of ξ . At *rate* = 2, **Algorithm 3** is stable up to $\xi = 38$. At *rate* = 3, 4 and 5, it is stable for all tested values of ξ . Compared with **Algorithm 2**, **Algorithm 3** possesses better stability and accuracy.

That relative errors keep decreasing as ξ increases up to 27 and increasing as ξ increases from 33 complies with the intuition mentioned in **Section 1**. It is guessed the amount of force added to the algorithm by taking ξ between 27 and 33 is close to the actual amount of

force resulting from added-mass effect in the coupling system.

9 A possible and non-rigorous explanation for the behaviour of stability

Theoretical analysis is not available yet. Here states a possible and non-rigorous explanation. It remains unknown whether such an explanation is correct.

All algorithms mentioned lead to linear equations after space discretizations at each time step. Compared with Fernandez's two algorithms, **Algorithms 1-3** modify the right hand side of those linear equations generated, causing perturbations to the solutions. Since Fernandez's two algorithms are stable, it is expected solutions still exist and do not change obviously under small perturbations. However, as β, θ or ξ increases, such perturbations become more significant and affect the existence and values of solutions more seriously. As time steps go on, perturbations accumulate and at some time steps cause the solutions to the linear equations generated at that step non-existent. This perhaps explains why **Algorithms 1-3** become unstable at large β, θ or ξ for a specific refinement *rate*.

For a specific value of β, θ or ξ , as the refinement *rate* increases, the number of nodes of mesh enlarges. Let an integer m denote the number of nodes on Σ , $m = L/h + 1$. The number of nodes on Ω is approximately m^2 . Note that the added force is only imposed on the interface. Thus, only m nodes are affected. The ratio of affected and non-affected nodes is approximately $m/(m^2 - m) = 1/(m - 1)$, which decreases as m increases. As refinement *rate* increases, m increases and therefore the forces added to **Algorithms 1-3** disturbs the system less, which yields better stability.

10 Selection of β, θ and ξ for practical applications

Practical applications should take into account both efficiency and accuracy. At refinement *rate* = 2, time step $\tau = 0.000125$, space discretization parameter $h = 0.025$, it takes no more than 20 seconds to finish computation for any of Fernandez's two algorithms and **Algorithms 1-3** regardless of values of β, θ and ξ . It is quite fast. However, all of them are far from

accurate. Therefore, practical applications are not expected to run at such low *rate* of refinement; it suffices to consider $rate = 3, 4$ and 5 .

Comparing relative errors corresponding to different values at $rate = 3, 4$ and 5 , the values $\beta = 43, \theta = 25, 31 \leq \xi \leq 33$ are recommended for **Algorithm 1-3** respectively. Tables 4, 5 and 6 report their values and percents of decrement of relative errors compared with Fernandez's algorithms respectively. The values of decrement of relative errors equal to relative errors of Fernandez's algorithms minus that of **Algorithm 1-3**, while percents equal to values divided by relative errors of Fernandez's algorithms times 100. Structure displacements are displayed in Figures 2, 3, 4, 5 and 6.

Table 4: Numerical results of Fernandez Explicit Robin-Neumann scheme (Fern ERN) and Algorithm 1 (Algo 1) at selected β

rate	Fern ERN	decrement of errors		
		$\beta = 43$	values	percents(%)
2	0.435176	unstable	N/A	N/A
3	0.241766	0.203850	0.037916	15.6829
4	0.128616	0.103949	0.024667	19.1788
5	0.064847	0.050604	0.014243	21.9640

Table 5: Numerical results of Fernandez fully decoupled scheme (Fern FD) and Algorithm 2 (Algo 2) at selected θ

rate	Fern FD	decrement of errors		
		$\theta = 25$	values	percents(%)
2	0.437713	unstable	N/A	N/A
3	0.243562	0.208879	0.034683	14.2399
4	0.129731	0.112158	0.017573	13.5457
5	0.065497	0.058477	0.00702	10.7180

Table 6: Numerical results of Fernandez fully decoupled scheme (Fern FD) and Algorithm 3 (Algo 3) at selected ξ

rate	Fern FD	Algo 3	decrement of errors	
			values	percents(%)
		$\xi = 31$		
2	0.437713	0.360862	0.076851	17.5574
3	0.243562	0.182757	0.060805	24.9649
4	0.129731	0.079329	0.050402	38.8512
5	0.065497	0.033437	0.03206	48.9488

rate	Fern FD	Algo 3	decrement of errors	
			values	percents(%)
		$\xi = 32$		
2	0.437713	0.363169	0.074544	17.0303
3	0.243562	0.183065	0.060497	24.8384
4	0.129731	0.078857	0.050874	39.2150
5	0.065497	0.033131	0.032366	49.4160

rate	Fern FD	Algo 3	decrement of errors	
			values	percents(%)
		$\xi = 33$		
2	0.437713	0.366107	0.071606	16.3591
3	0.243562	0.183835	0.059727	24.5223
4	0.129731	0.078730	0.051001	39.3129
5	0.065497	0.033061	0.032436	49.5229

Not applicable

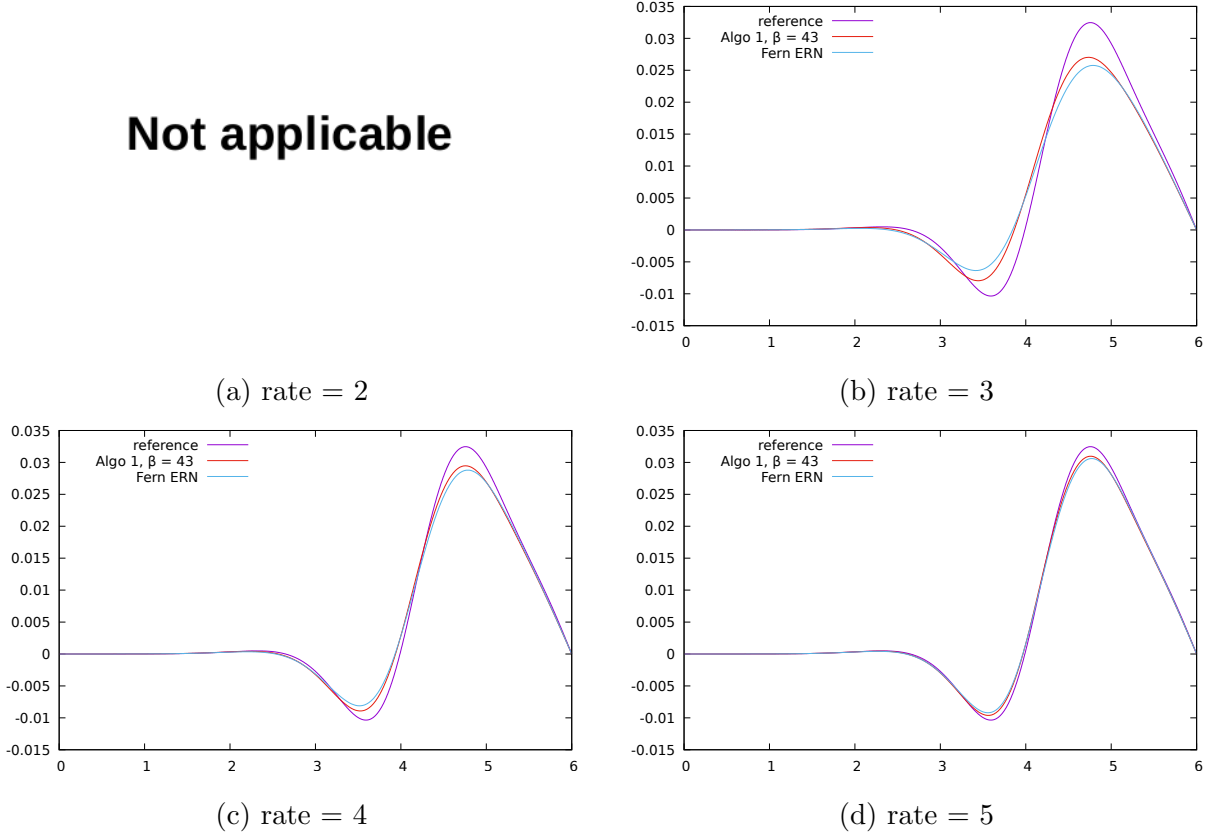


Figure 2: Structure displacement of Fernandez Explicit Robin-Neumann scheme (Fern ERN) and Algorithm 1 (Algo 1) with $\beta = 43$ at final time

11 Discussions and future work

The numerical results validate the ideas that adding force corresponding to viscosity and replacing underlying projection method can improve accuracy; particularly, Table 6 indicates as large improvement as up to 49.5229% for **Algorithm 3** with $\xi = 33$ compared with **Fernandez fully decoupled scheme** at refinement $rate = 5$. It is expected, for other fluid-structure interaction problems, if the fluid is also viscous, adding force might also help with accuracy.

As a direction of future work, it is worth trying investigating how adding force improve accuracy theoretically. Reading works [4] [3] on added-mass effect might benefit such analysis.

This work deals with accuracy. On the other hand, it is possible to improve efficiency by

Not applicable

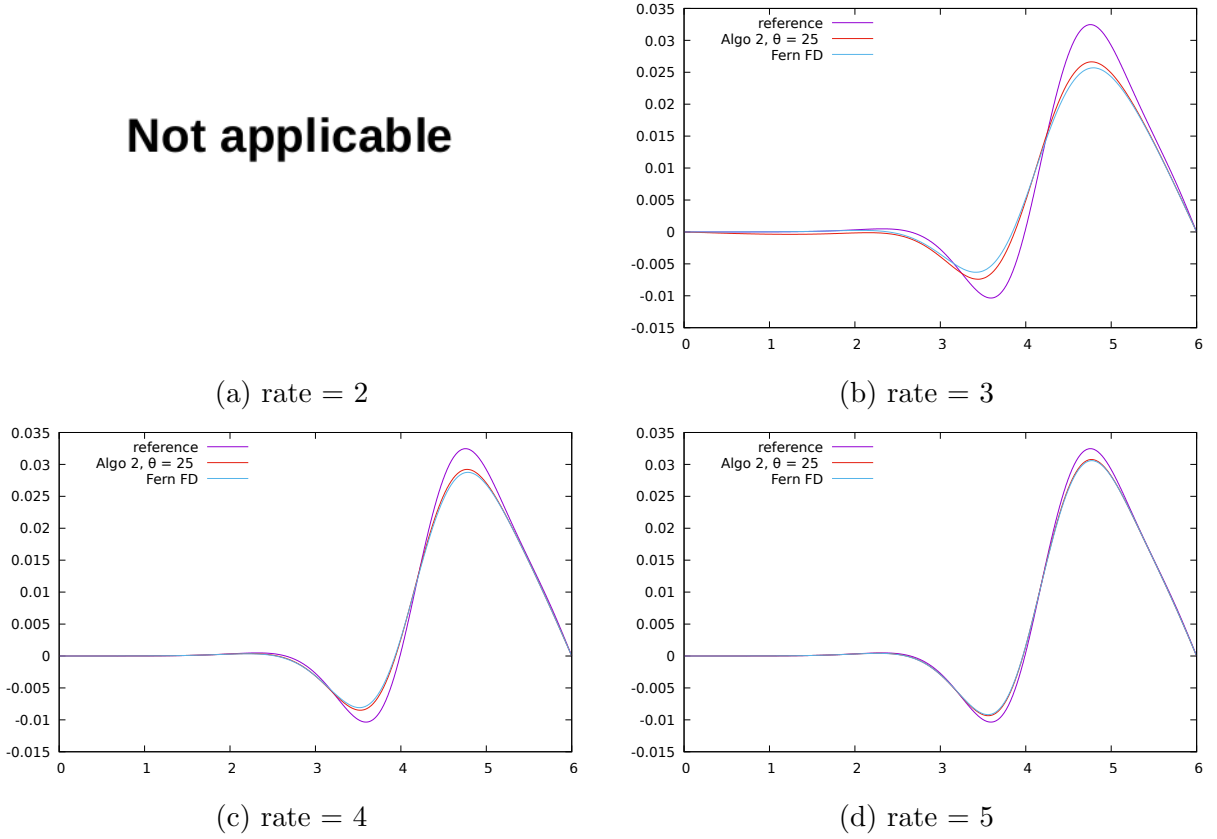


Figure 3: Structure displacement of Fernandez fully decoupled scheme (Fern FD) and Algorithm 2 (Algo 2) with $\theta = 25$ at final time

parallelism. A choice is to take advantage of extrapolation (1^{st} order might be better than 0^{th}). To implement such ideas, MPI [1] might work.

12 Acknowledgments

This research did not receive any specific grant from funding agencies in the public, commercial, or not-for-profit sectors.

The proposal of ideas as well as algorithms, numerical experiments, conclusions, explanations and draft of this article are completed entirely independently, without any assistance or guide from anyone else.

This article serves as the author's PhD thesis. Compared with the draft written before Thesis Exam held on August 10 2020, this is a revised version. The Thesis Examination Committee (consisting of Prof. Mo MU, Prof. Jian-Feng CAI, Prof. Kun XU, Prof. Eric

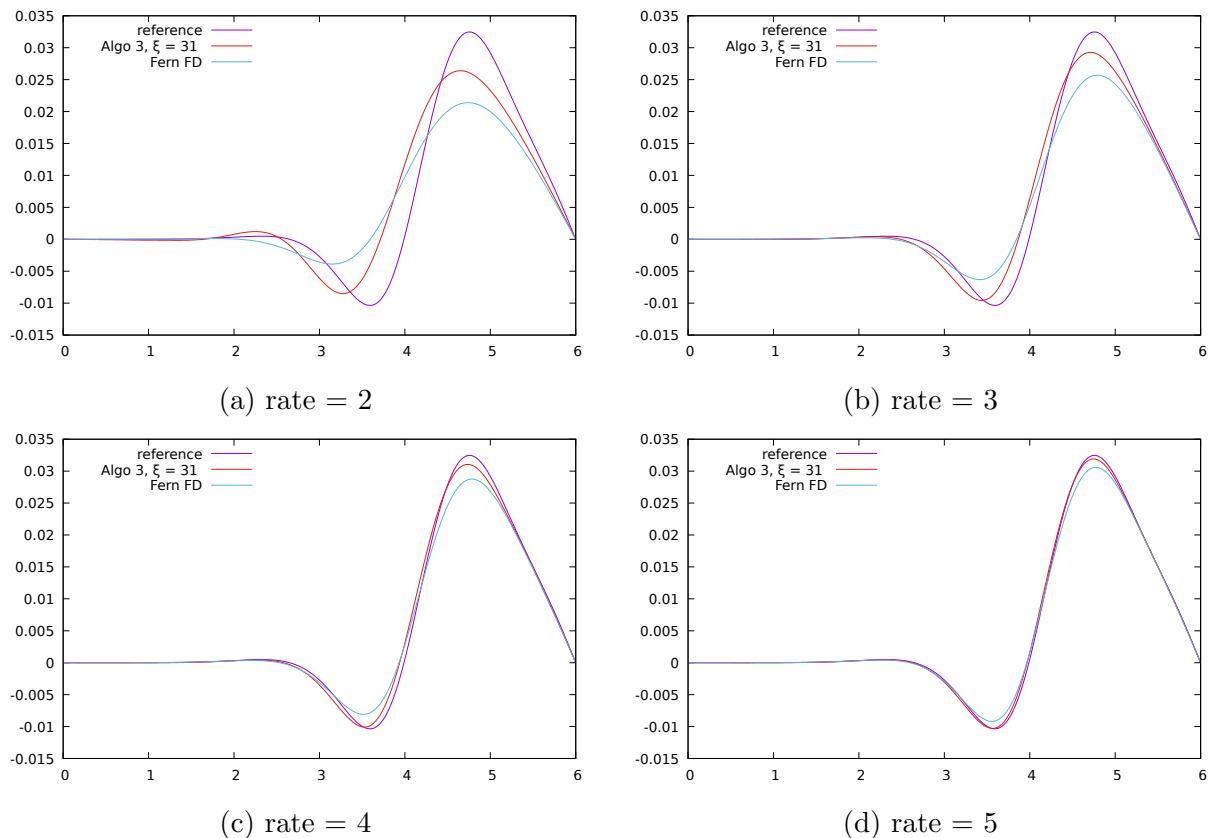
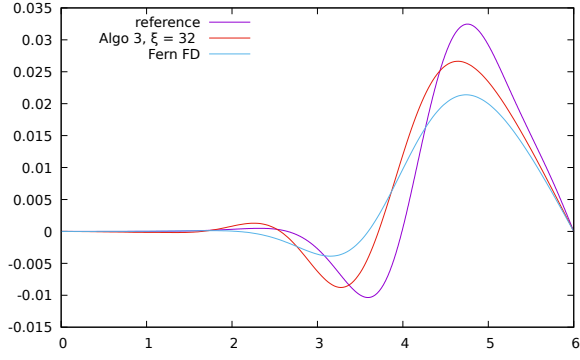
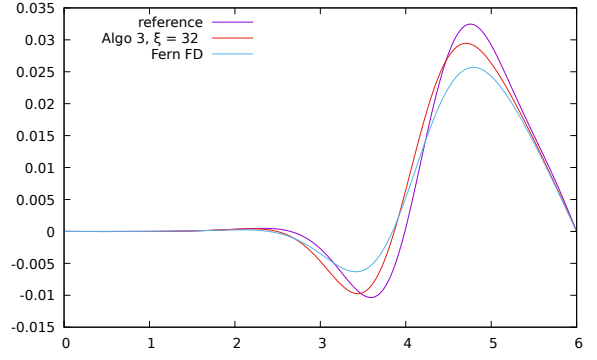


Figure 4: Structure displacement of Fernandez fully decoupled scheme (Fern FD) and Algorithm 3 (Algo 3) with $\xi = 31$ at final time

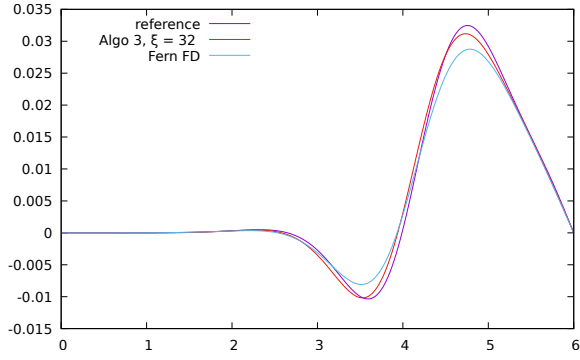
Tsz Shun CHUNG, Prof. Jidong ZHAO and Prof. Jensen Tsan Hang LI), especially Prof. Mo MU, advised on the writing and provides lots of very useful suggestions, precisely on the writing of Sections 1, 8 and 9 after the Thesis Exam. The author greatly appreciates their advices.



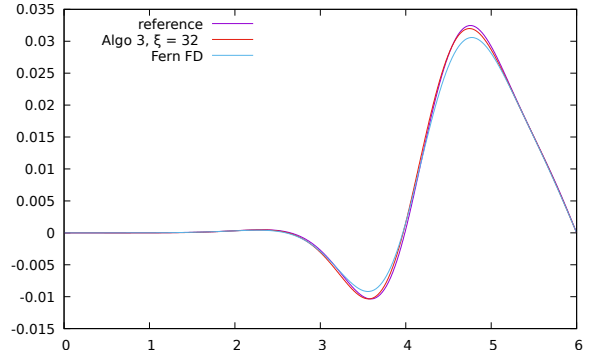
(a) rate = 2



(b) rate = 3

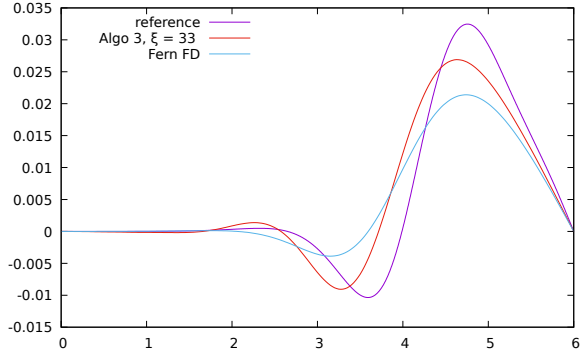


(c) rate = 4

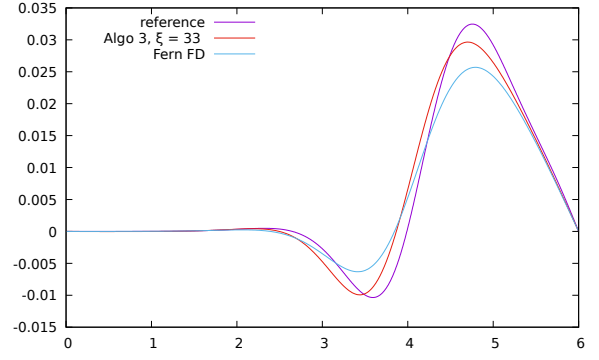


(d) rate = 5

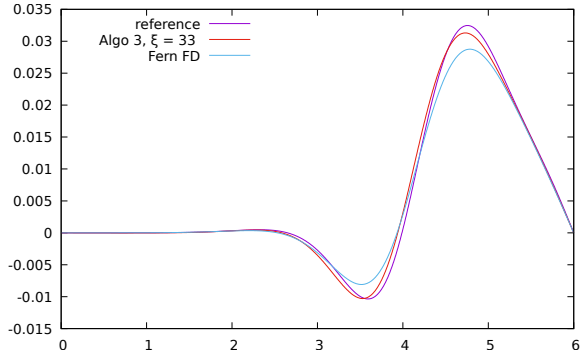
Figure 5: Structure displacement of Fernandez fully decoupled scheme (Fern FD) and Algorithm 3 (Algo 3) with $\xi = 32$ at final time



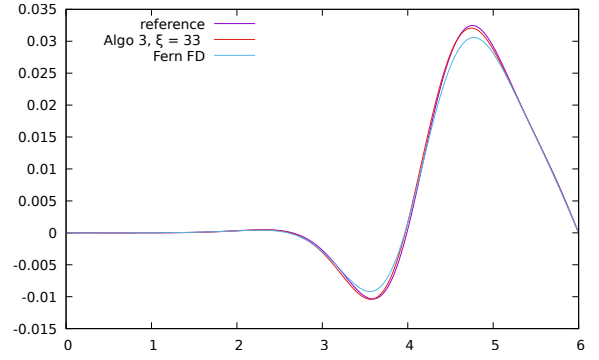
(a) rate = 2



(b) rate = 3



(c) rate = 4



(d) rate = 5

Figure 6: Structure displacement of Fernandez fully decoupled scheme (Fern FD) and Algorithm 3 (Algo 3) with $\xi = 33$ at final time

References

- [1] Blaise Barney. Message passing interface (mpi). <https://computing.llnl.gov/tutorials/mpi/>. Accessed June 01 2019.
- [2] Pitkäranta J Brezzi F. On the stabilization of finite element approximations of the stokes equations. *Efficient Solutions of Elliptic Systems (Kiel, 1984), Notes on Numerical Fluid Mechanics*, 10:11–19, 1984.
- [3] Suncica Canic, Boris Muha, and Martina Bukac. Stability of the kinematically coupled beta-scheme for fluid-structure interaction problems in hemodynamics. *INTERNATIONAL JOURNAL OF NUMERICAL ANALYSIS AND MODELING*, 12(1):54–80, 2012.
- [4] P. Causin, J.F. Gerbeau, and F. Nobile. Added-mass effect in the design of partitioned algorithms for fluid–structure problems. *Computer Methods in Applied Mechanics and Engineering*, 194(42):4506 – 4527, 2005.
- [5] Miguel A. Fernandez. Fsi lectures tutorial 2: Robust and accurate splitting schemes. November 9-13, 2015, IST, Lisbon, Portugal.
- [6] M.A. Fernández and M. Landajuela. A fully decoupled scheme for the interaction of a thin-walled structure with an incompressible fluid. *Comptes Rendus Mathématique*, 351(3-4):161–164, 2013.
- [7] Miguel A Fernández and Mikel Landajuela. Splitting schemes for incompressible fluid/thin-walled structure interaction with unfitted meshes. *Comptes rendus - Mathématique*, 353(7):647–652, 2015.
- [8] Miguel A. Fernández, Mikel Landajuela, and Marina Vidrascu. Fully decoupled time-marching schemes for incompressible fluid/thin-walled structure interaction. *Journal of Computational Physics*, 297(C):156–181, 2015.

- [9] Miguel A. Fernández, Jimmy Mullaert, and Marina Vidrascu. Explicit robin-neumann schemes for the coupling of incompressible fluids with thin-walled structures. *Computer Methods in Applied Mechanics and Engineering*, 267:566 – 593, 2013.
- [10] Luca Formaggia, Alfio Quarteroni, and Allesandro Veneziani. *Cardiovascular Mathematics: Modeling and simulation of the circulatory system*. Springer Milan : Imprint: Springer, Milano, 1st ed.. edition, 2009.
- [11] Brian Fox and Chet Ramey. Gnu bash. <https://www.gnu.org/software/bash/>. GNU Bash 4.4 August 26 2016.
- [12] Jean-Frédéric Gerbeau and Marina Vidrascu. A quasi-newton algorithm based on a reduced model for fluid-structure interaction problems in blood flows. *ESAIM. Mathematical modelling and numerical analysis*, 37(4):631–647, 2003.
- [13] J.L. Guermond, P. Mineev, and Jie Shen. An overview of projection methods for incompressible flows. *Computer Methods in Applied Mechanics and Engineering*, 195(44-47):6011–6045, 2006.
- [14] Sang Truong Ha, Long Cu Ngo, Muhammad Saeed, Byoung Jin Jeon, and Hyounggwon Choi. A comparative study between partitioned and monolithic methods for the problems with 3d fluid-structure interaction of blood vessels. *Journal of Mechanical Science and Technology*, 31(1):281–287, 2017.
- [15] F. Hecht. New development in freefem++. *J. Numer. Math.*, 20(3-4):251–265, 2012.
- [16] Dmitri Kuzmin. Operator splitting techniques. <http://www.mathematik.uni-dortmund.de/~kuzmin/cfdintro/lecture11.pdf>. Accessed August 1 2018.
- [17] A lot of contributors. Comprehensive perl archive network. <https://www.cpan.org/>. Accessed June 06 2020.
- [18] Fabio Nobile. Numerical approximation of fluid-structure interaction problems with application to haemodynamics. page 203, 2001.

- [19] Linus Torvalds and a huge number of contributors. The linux kernel archives. <https://www.kernel.org/>. Accessed June 07 2020.
- [20] Larry Wall and the help of oodles of other folks. The perl programming language. <https://www.perl.org/>. Perl v5.30.0 April 17 2020.
- [21] Thomas Williams, Colin Kelley, and a large number of contributors on SourceForge. Gnuplot. <http://www.gnuplot.info/>. Gnuplot v5.0.16(1)-release (x86_64-pc-linux-gnu) 4th Berkeley Distribution March 15 2019.